Geophysical Research Letters

RESEARCH LETTER
10.1029/2020GL090037

Special Section:
The COVID-19 Pandemic: Linking Health, Society and Environment

Observed Impacts of COVID-19 on Urban CO_2 Emissions

Alexander J. Turner[1,2,3,4], Jinsol Kim[1], Helen Fitzmaurice[1], Catherine Newman[2], Kevin Worthington[2], Katherine Chan[2], Paul J. Wooldridge[2], Philipp Köehler[5], Christian Frankenberg[3,5], and Ronald C. Cohen[1,2]

[1]Department of Earth and Planetary Sciences, University of California, Berkeley, CA, USA, [2]College of Chemistry, University of California, Berkeley, CA, USA, [3]Jet Propulsion Laboratory, California Institute of Technology, Pasadena, CA, USA, [4]Now at Department of Atmospheric Sciences, University of Washington, Seattle, WA, USA, [5]Division of Geological and Planetary Sciences, California Institute of Technology, Pasadena, CA, USA

Abstract Governments restricted mobility and effectively shuttered much of the global economy in response to the COVID-19 pandemic. Six San Francisco Bay Area counties were the first region in the United States to issue a "shelter-in-place" order asking non-essential workers to stay home. Here we use CO_2 observations from 35 Berkeley Environment, Air-quality and CO_2 Network ($BEACO_2N$) nodes and an atmospheric transport model to quantify changes in urban CO_2 emissions due to the order. We infer hourly emissions at 900-m spatial resolution for 6 weeks before and 6 weeks during the order. We observe a 30% decrease in anthropogenic CO_2 emissions during the order and show that this decrease is primarily due to changes in traffic (−48%) with pronounced changes to daily and weekly cycles; non-traffic emissions show small changes (−8%). These findings provide a glimpse into a future with reduced CO_2 emissions through electrification of vehicles.

Plain Language Summary This work uses atmospheric observations to quantify the changes in urban CO_2 emissions from different sectors in response to COVID-19 mobility regulations.

Key Points:
- A 30% decrease in urban CO_2 emissions was observed from the San Francisco Bay Area in response to COVID-19 mobility restrictions
- Changes are primarily driven by a decrease in CO_2 emissions from traffic (−48%)
- There is a large change to the weekly and diurnal cycle of emissions with reductions in morning rush hour emissions

Supporting Information:
- Supporting Information S1

Correspondence to:
R. C. Cohen,
rccohen@berkeley.edu

Citation:
Turner, A. J., Kim, J., Fitzmaurice, H., Newman, C., Worthington, K., Chan, K., et. al. (2020). Observed impacts of COVID-19 on urban CO_2 emissions. *Geophysical Research Letters*, *47*, e2020GL090037. https://doi.org/10.1029/2020GL090037

Received 24 JUL 2020
Accepted 27 OCT 2020
Accepted article online 30 OCT 2020

1. Introduction

Carbon dioxide (CO_2) is an atmospheric trace gas responsible for most of the growth in anthropogenic radiative forcing (IPCC, 2013). Mitigating long-term climate change necessitates drastic reductions to our CO_2 emissions. Specifically, limiting global mean warming to 1.5°C requires reaching net-zero anthropogenic CO_2 emissions by 2050 (IPCC, 2018). Over 70% of these anthropogenic CO_2 emissions in the United States are attributable to urban areas (EIA, 2015; Hutyra et al., 2014); as such, it is important to be able to accurately quantify the emissions from these regions to support regulatory policies aimed at CO_2 reduction and provide citizens with metrics indicating their effectiveness.

The abrupt shuttering of the global economy in response to the COVID-19 global pandemic presents an opportunity to evaluate methods for quantifying urban CO_2 emissions, to assess our ability to attribute emissions to specific source sectors, and to describe the changes in emissions from different sectors. Understanding the changes that occurred during the COVID-19 period will allow us to identify (1) the magnitude and subset of CO_2 emissions that respond to changes in our travel to/from workplaces on short time scales and (2) the sectors whose emissions persist irrespective of changes in urban travel patterns. Recent research used changes in activity data to predict the impact of COVID-19 on global CO_2 emissions and inferred a −17% (−11% to −25%) change in global daily CO_2 emissions (Le Quéré et al., 2020). This prediction has yet to be confirmed with measurements of atmospheric CO_2.

The focus of this study is the San Francisco Bay Area in Northern California as it was the first region in the United States to enact regulations on mobility through a "shelter-in-place" (SIP) order on 16 March 2020 (Contra Costa County Health Officer, 2020). We use a dense network of CO_2 observations across the north eastern region of the San Francisco Bay Area to quantify the impacts of the SIP order on urban CO_2 emissions. Figure 1a shows the spatial coverage of our ground-based network of in situ sensors: the Berkeley Environmental Air-quality and CO_2 Network ($BEACO_2N$; Shusterman et al., 2016; Turner et al., 2016; Shusterman et al., 2018; Kim et al., 2018). Shusterman et al. (2016) and Text S1 give additional details on the

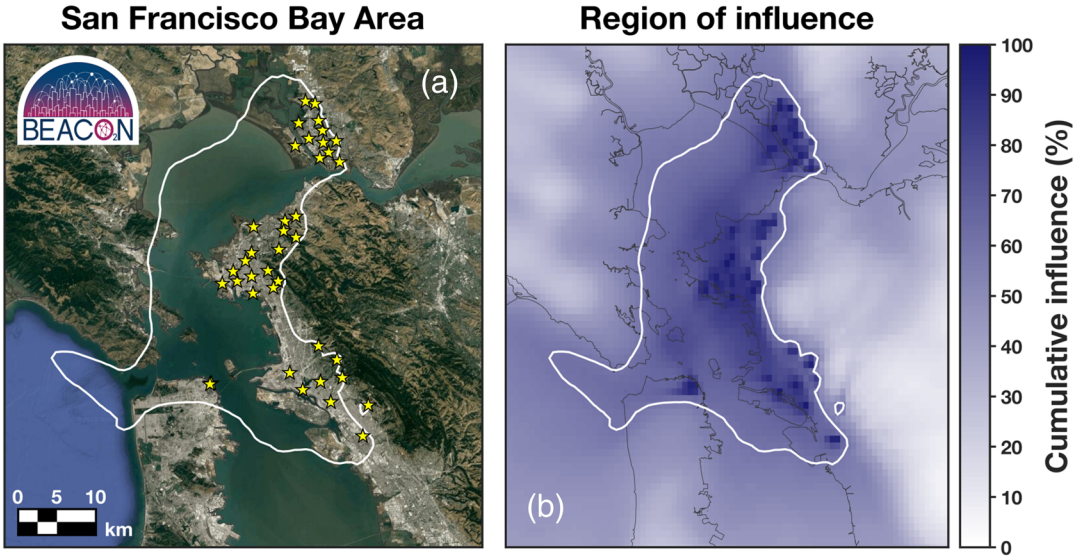

Figure 1. Observational network in the San Francisco Bay Area. Panel (a) shows the location of instruments in the Berkeley Environmental Air-quality and CO_2 Network ($BEACO_2N$; yellow stars). Panel (b) shows the cumulative influence to the network derived from STILT footprints for observations in March 2020. White contour in both panels indicates the region that contains the largest 40% of the total network influence (referred to as the "$BEACO_2N$ Domain").

network. We examine data from the study period between 2 February 2020 and 2 May 2020, during which 35 sensors were operational.

2. Atmospheric Inversion Framework

Figure 2 shows a comparison of the network-wide median CO_2 concentrations for each day-of-week for 6 weeks before and during the SIP order. We observe a 5–50 ppm decrease in midweek CO_2 concentrations with the most pronounced changes on Monday through Thursday during the morning rush hour (~07:00 local time). Weekend concentrations show small differences in the median between the two time periods, although the variability is somewhat larger before the SIP. These observations suggest that (1) large reductions in CO_2 emissions occurred due to the SIP order and (2) marked changes to both the daily and weekly cycle of emissions due to shifts in human activity. Quantifying and attributing changes in CO_2 concentrations to emissions require accounting for the coupling of meteorology and emissions.

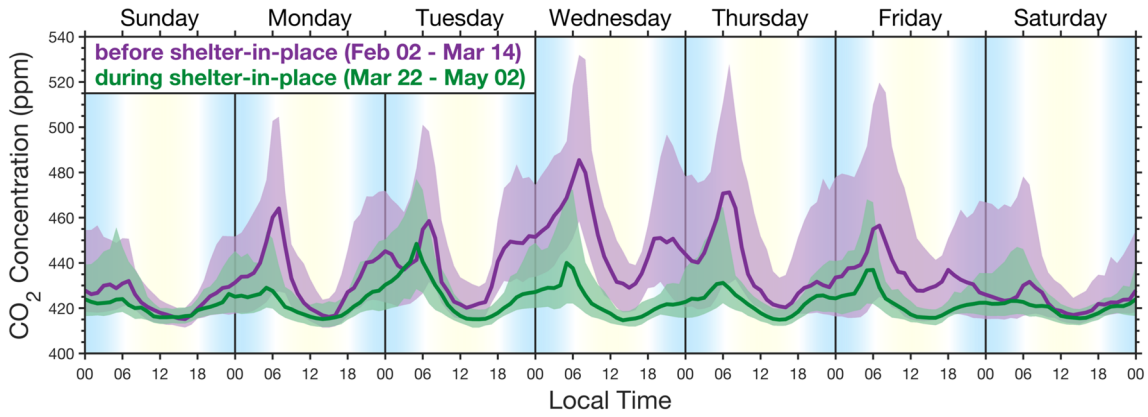

Figure 2. Weekly CO_2 concentrations before and during shelter-in-place order. Solid lines show the median across the $BEACO_2N$ network and the shaded region indicates the 16th to 84th percentile. Purple shows 6 weeks of data before shelter-in-place (2 February 2020 through 14 March 2020) and green is 6 weeks during shelter-in-place (22 March 2020 through 2 May 2020). Blue/yellow background shading is based on cosine of the solar zenith angle with white indicating dawn and dusk.

We use the Stochastic Time-Inverted Lagrangian Transport model (STILT; Fasoli et al., 2018; Lin et al., 2003) with meteorology from the NOAA High-Resolution Rapid Refresh (HRRR Kenyon et al., 2016) to both estimate the sensitivity of each measurement to upwind emission sources and estimate the concentration upwind of our domain. Text S2 provides details on the transport modeling. Each measurement (y_i) has a unique background concentration (b_i; see Text S3) and footprint ($\mathbf{h}_i$). The footprint represents the spatiotemporal region that an atmospheric measurement is sensitive to (i.e., the region that could influence a measurement; see Fasoli et al., 2018; Lin et al., 2003; and Turner et al., 2016, 2018, for additional details on constructing the footprints).

The measurements are related to the surface CO_2 emissions ($\mathbf{x}$) as $y_i = \mathbf{h}_i\mathbf{x} + b_i$, and we use Bayesian inference to obtain hourly CO_2 emissions at 900-m spatial resolution from the atmospheric measurements. Prior fluxes are adapted from previous work (McDonald et al., 2014; Turner et al., 2016) but now use a biosphere derived from measurements of solar-induced chlorophyll fluorescence (SIF; Turner et al., 2020). Additionally, we manually inspected the 20 largest point sources to ensure they were spatially allocated to plausible locations. Errors are assumed to be Gaussian and include off-diagonal terms in both error covariance matrices. Following Rodgers (1990), we solve for the hourly posterior fluxes at 900-m spatial resolution as

$$\hat{\mathbf{x}} = \mathbf{x_a} + (\mathbf{HB})^T(\mathbf{HBH}^T + \mathbf{R})^{-1}(\mathbf{y} - \mathbf{Hx_a}) \quad (1)$$

where $\hat{\mathbf{x}}$ ($m \times 1$) is the posterior fluxes, x_a ($m \times 1$) is the prior emissions, $\mathbf{y}$ ($n \times 1$) is the $BEACO_2N$ observations, $\mathbf{H}$ ($n \times m$) is the matrix of footprints from HRRR-STILT, $\mathbf{R}$ ($n \times n$) is the model-data mismatch error covariance matrix, and $\mathbf{B}$ ($m \times m$) is the prior error covariance matrix (see Text S4 for additional details).

Posterior fluxes will reflect the prior fluxes in regions with low sensitivity from the measurements. This can be clearly seen by looking at Equation 1 and the gain matrix: $\mathbf{G} = (\mathbf{HB})^T(\mathbf{HBH}^T + \mathbf{R})^{-1}$. We can see that $\hat{\mathbf{x}} \rightarrow \mathbf{x_a}$ in Equation 1 as $\mathbf{G} \rightarrow \mathbf{0}$, indicating that our posterior solution will not deviate from the prior in regions of low sensitivity. As such, we focus our study on regions with high sensitivity because those are the regions that our observations can robustly constrain. Figure 1b shows the region of influence for the $BEACO_2N$ network. We find the network to be most sensitive to the eastern portion of the San Francisco Bay Area with upwind influence extending east across the bay to San Francisco. The white contour in Figure 1b encapsulates the top 40% of the total of the network sensitivity, hereafter referred to as the "$BEACO_2N$ Domain," where we expect strong constraints from the measurements.

3. High-Resolution Posterior Fluxes

The resulting posterior fluxes inferred using $BEACO_2N$ observations are shown in Figure 3. Figures 3a and 3b show the spatial patterns before and during the SIP order, respectively, while Figure 3c shows the difference. Changes on roadways are evident in the pattern of differences. Changes to other sectors are more subtle. We have high confidence in the fluxes within the $BEACO_2N$ Domain because this is the region where the $BEACO_2N$ network is strongly sensitive to; fluxes outside of this region will revert to the prior emissions. Two spatial features that immediately stand out in Figure 3c are a 0.4 $tC\,km^{-2}\,hr^{-1}$ decrease in emissions over urban areas within the $BEACO_2N$ Domain and a modest decrease (0.15 $tC\,km^{-2}\,hr^{-1}$) across most of the San Francisco Bay Area. We are able to attribute these observed changes to particular sectors because of the (1) high spatial resolution obtained here, (2) satellite observations to constrain the biosphere, and (3) detailed prior information available in the region. We find that the modest regional decrease is due to the biosphere and the large changes in urban areas are predominantly due to decreases in traffic.

Estimating CO_2 fluxes from observations during spring is complicated by the onset of photosynthesis which results in a decrease in atmospheric concentrations. In Northern California, this begins with the grasslands and chaparral in land surrounding the urban core. As mentioned above, we use high-resolution satellite observations of SIF from TROPOMI to constrain the biospheric activity during this time of year (Turner et al., 2020), which have been shown to correlate strongly with photosynthetic activity (e.g., Frankenberg et al., 2011; Yang et al., 2015; and others). These space-borne SIF measurements indicate a 170% (37 tC/hr) increase in daytime CO_2 uptake from the biosphere across the $BEACO_2N$ Domain when comparing before and during the SIP order. This increase in biospheric activity inferred from space-borne SIF measurements drives the regional decrease in CO_2 fluxes shown in Figure 3c.

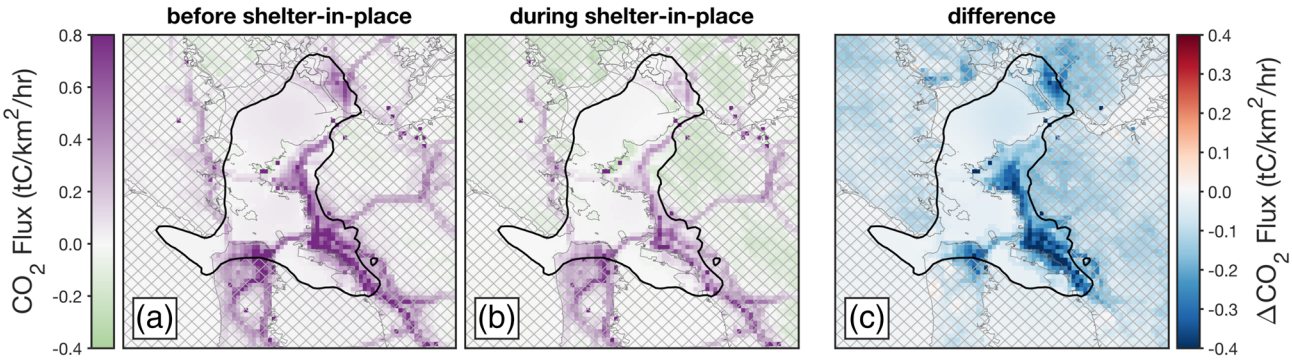

Figure 3. Spatial patterns of CO_2 fluxes in the San Francisco Bay Area. Panel (a) shows the average CO_2 fluxes for 6 weeks before shelter-in-place (2 February 2020 through 14 March 2020). Panel (b) shows the average over 6 weeks during shelter-in-place (22 March 2020 through 2 May 2020). Panel (c) is the difference. Black contour in all panels encompasses the top 40% of the total network influence ($BEACO_2N$ Domain). Cross hatching indicates regions with low sensitivity to the $BEACO_2N$ nodes.

The large changes within the $BEACO_2N$ Domain coincide with major freeways in the San Francisco Bay Area. In particular, the largest decreases are observed over Interstate 880 (I-880) that runs north–south from San Jose to Oakland. Our observational network is only sensitive to the northern half of I-880, but the entirety of that section shows decreases in CO_2 fluxes in excess of 0.4 tC km^{-2} hr^{-1}. I-880 is a crucial freeway for workers commuting to San Francisco. Other freeways that serve commuters also show large decreases in CO_2 fluxes (e.g., Interstates 80 and 580).

Figure 4 shows the posterior CO_2 emissions within the $BEACO_2N$ Domain before and during the SIP order. In toto, we observe a 39% decrease in CO_2 fluxes between the two time periods. However, the most striking feature is the large perturbation to both the daily and weekly cycle of CO_2 fluxes. We observe large CO_2 fluxes that are coincident with rush hour before the SIP order. These features are largely absent during the SIP order. The pronounced changes in the daily cycle found here highlight the importance of incorporating measurements over the course of the day, rather than just the well-mixed afternoon as is often done.

A common method of characterizing errors in flux inversions is to examine the posterior error covariance matrix: $\mathbf{Q} = (\mathbf{H}^T\mathbf{R}^{-1}\mathbf{H} + \mathbf{B}^{-1})^{-1}$. However, $\mathbf{Q}$ would have in excess of 10^{13} elements here and, assuming single precision, require more than 180 Tb to store. As such, $\mathbf{Q}$ is computationally intractable. We instead adopt two methods of characterizing the uncertainty: (1) examination of the day-to-day variation and (2) k-fold cross validation. The shaded regions in Figure 4 show the 1-σ spread in CO_2 fluxes for given hour of the week (i.e., the variation across the 6 weeks). The cross validation is shown in Text S7 where we find the posterior fluxes to explain 23% more variability than the prior fluxes when compared against observations withheld from the flux inversion. There is ongoing work comparing these results against independent data of traffic flow from the California Department of Transportation (Caltrans, 2020).

In our work, we solve for total CO_2 fluxes. However, we leverage the high spatial resolution obtained here to partition our posterior CO_2 fluxes to specific sectors because sources spatially separate as the resolution increases. For example, McDonald et al. (2014) demonstrated that 1-km spatial resolution was necessary to distinguish freeways from arterial roads. Here, we classify grid cells that have the majority of prior emissions coming from a single sector (e.g., we classify a grid cell as "traffic" if more than 50% of the prior emissions come from the traffic sector; see Text S5 for more details).

Figure 4 attributes the posterior CO_2 emissions within the $BEACO_2N$ Domain to three sectors: (1) vehicle traffic, (2) stationary anthropogenic emissions, and (3) biogenic. Over 80% of the emissions from the stationary sector are due to the industrial point sources which likely have small variations over the diurnal cycle. We observe the highest CO_2 emissions during the morning rush hour in the middle of the week. This peak is only present during the weekdays. Daily average emissions increase from Sunday to their maximum on Wednesday and then decrease from Wednesday to Saturday. In contrast, daily average emissions during SIP have more subtle differences between weekdays and weekends, as suggested by the day of week variation in the concentrations of CO_2 shown in Figure 2. Weekday emissions start earlier than on weekends before and after the SIP order. After the SIP, rush hour emissions are lower, but they still extend emissions earlier and later than seen on weekends, resulting in a flatter weekday daytime emissions profile than on weekends.

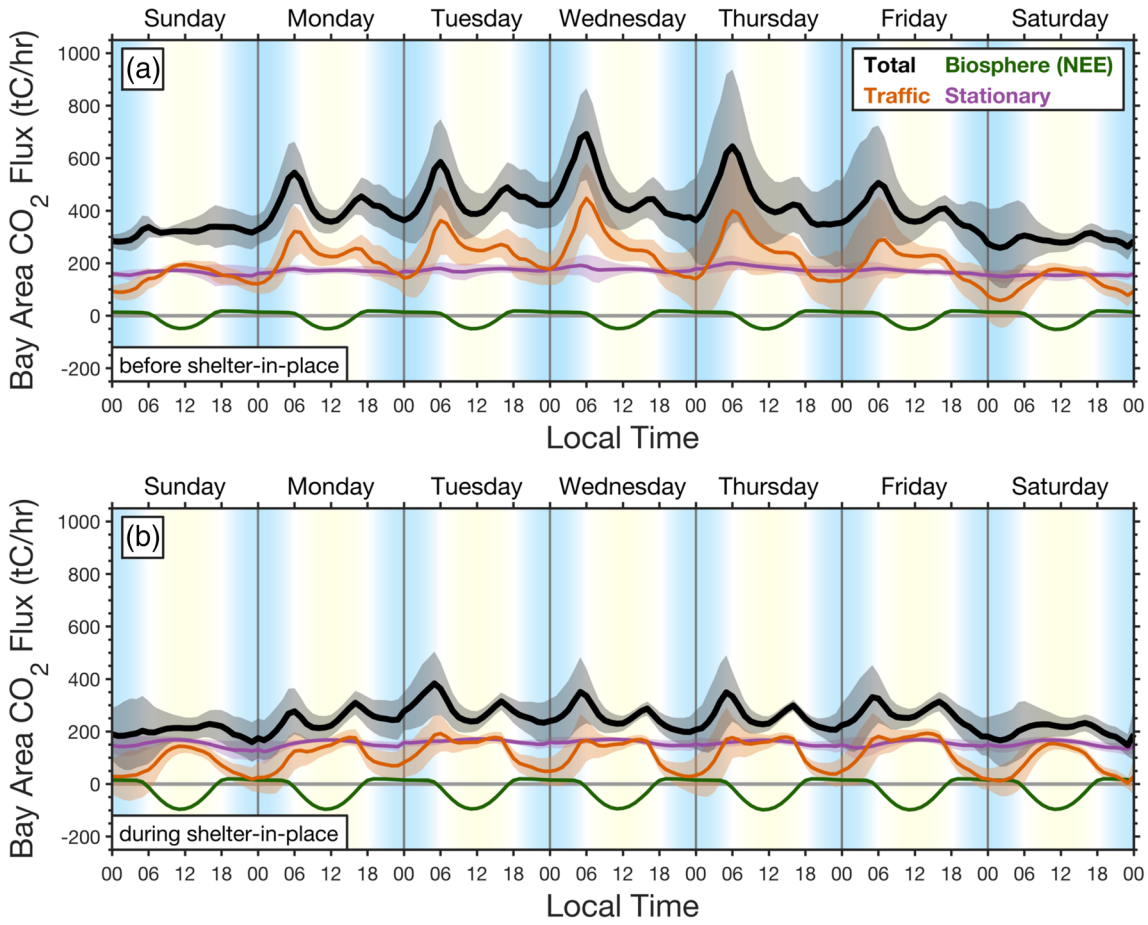

Figure 4. Weekly cycle of CO_2 fluxes before and during shelter-in-place order. Solid lines are the weekly mean CO_2 fluxes over the BEACO$_2$N Domain (top 40th percentile shown in Figure 1) and shading is 1-σ. Black are the total fluxes. Orange are the traffic emissions. Purple are stationary anthropogenic sources such as industrial point sources, residential heating, and other non-vehicle anthropogenic sources. Green are the biosphere fluxes (net ecosystem exchange [NEE]). Panel (a) shows emissions before shelter-in-place (2 February 2020 through 14 March 2020) and panel (b) shows emissions during shelter-in-place (22 March 2020 through 2 May 2020).

We find that grid cells classified as stationary sources decreased by 8% (–14 tC/hr) in response to the SIP order. The posterior emissions indicate a small diurnal cycle in the stationary sector that is largely absent before the SIP order and is not present in the prior emissions. In contrast, we find a –48% change (–97 tC/hr) in the weekly average CO_2 emissions from grid cells that are classified as freeway whereas emissions. Emissions from vehicles at night pre-SIP averaged ~154 tC/hr and during SIP the nighttime emissions averaged ~55 tC/hr. This represents a 64% decrease in nighttime emissions and a 40% decrease during daytime (240 to 144 tC/hr). Independent data from the California Department of Transportation also indicate a 41% and 34% decrease in vehicle miles traveled by cars and trucks, respectively, for road segments in the BEACO$_2$N Domain (Caltrans, 2020).

On weekdays before the SIP order, vehicles are the largest source of CO_2 during daytime, while on pre-SIP weekends, stationary and traffic sources have a comparable magnitude. After the SIP order, stationary sources are generally the largest term. Such sectoral changes are possible to observe here due to the densely spaced nodes in the BEACO$_2$N network, allowing us to obtain subkilometer spatial resolution and resolve different sectors.

4. Conclusions

This unnatural experiment conducted in response to COVID-19 has demonstrated the subset of CO_2 emissions that are elastic and those that are more entrenched. Emissions from traffic are highly elastic and could be rapidly mitigated in response to either technological advances or regulations. In contrast, the stationary

emissions (e.g., industrial point sources and residential heating) showed minimal changes in response to the SIP order. This implies that those sources are more entrenched and will require longer time scales to mitigate if we hope to limit future warming. These findings provide a glimpse into a future where CO_2 emissions from vehicle traffic are reduced through the electrification of the vehicle fleet, which would also have air quality cobenefits; observing these CO_2 emission changes from such a transition will require sustained measurements as the changes will be more subtle than the abrupt 48% changes seen here.

Conflict of Interest

The authors declare no competing interests.

Data Availability Statement

CO_2 data are available online (http://beacon.berkeley.edu/). Code has been deposited in GitHub (https://www.github.com/alexjturner/UrbanInversion).

Acknowledgments
We thank B. Fasoli for recent developments to the STILT model and sharing pre-processing code, E. Delaria for developing a temperature calibration, P. Vannucci and A. Lall for feedback, and former members of the $BEACO_2N$ project for establishing the network: A. A. Shusterman, V. Teige, and K. Lieschke. The author acknowledges ideas and advice from the participants in the COVID-19 and Earth System Science workshop organized by the W.M. Keck Institute for Space Studies. We are grateful to the team that has realized the TROPOMI instrument, consisting of the partnership between Airbus Defence and Space, KNMI, SRON, and TNO, commissioned by NSO and ESA. A. J. T. was supported as a Miller Fellow with the Miller Institute for Basic Research in Science at UC Berkeley. This research was funded by grants from the Koret Foundation and University of California, Berkeley. Part of this research was funded by the NASA Carbon Cycle Science program (grant NNX17AE14G). TROPOMI SIF data generation by P. K. and C. F. is funded by the Earth Science U.S. Participating Investigator program (grant NNX15AH95G). This research used the Savio computational cluster resource provided by the Berkeley Research Computing program at the University of California, Berkeley (supported by the UC Berkeley Chancellor, Vice Chancellor for Research, and Chief Information Officer).

References

Caltrans (2020). *Performance Measurement System Data Source*. Sacramento, CA: California Department of Transportation. https://pems.dot.ca.gov

Contra Costa County Health Officer (2020). *Contra Costa County Shelter-in-Place Order*: Contra Costa County. Retrieved from https://cchealth.org/coronavirus/pdf/HO-COVID19-SIP-0316-2020.pdf

EIA (2015). Emissions of Greenhouse Gases in the U.S. (*Tech report*): U.S. Energy Information Administration.

Fasoli, B., Lin, J. C., Bowling, D. R., Mitchell, L., & Mendoza, D. (2018). Simulating atmospheric tracer concentrations for spatially distributed receptors: Updates to the Stochastic Time-Inverted Lagrangian Transport model's R interface (STILT-R version 2). *Geoscientific Model Development*, *11*(7), 2813–2824. https://doi.org/10.5194/gmd-11-2813-2018

Frankenberg, C., Fisher, J. B., Worden, J., Badgley, G., Saatchi, S. S., Lee, J. E., & Yokota, T. (2011). New global observations of the terrestrial carbon cycle from GOSAT: Patterns of plant fluorescence with gross primary productivity. *Geophysical Research Letters*, *38*, L17706. https://doi.org/10.1029/2011GL048738

Hutyra, L. R., Duren, R., Gurney, K. R., Grimm, N., Kort, E. A., Larson, E., & Shrestha, G. (2014). Urbanization and the carbon cycle: Current capabilities and research outlook from the natural sciences perspective. https://doi.org/10.1002/2014ef000255

IPCC (2013). Climate Change 2013: The Physical Science Basis. Contribution of Working Group I to the Fifth Assessment Report of the Intergovernmental Panel on Climate Change. (Tech. Rep.). Author.

IPCC (2018). Global Warming of 1.5°C. An IPCC Special Report on the impacts of global warming of 1.5°C above pre-industrial levels and related global greenhouse gas emission pathways, in the context of strengthening the global response to the threat of climate change, sustainable development, and efforts to eradicate poverty. (Tech. Rep.). Author.

Kenyon, J. S., Moninger, W. R., Smith, T. L., Peckham, S. E., Lin, H., Grell, G. A., & Manikin, G. S. (2016). A North American hourly assimilation and model forecast cycle: The Rapid Refresh. *Monthly Weather Review*, *144*(4), 1669–1694. https://doi.org/10.1175/mwr-d-15-0242.1

Kim, J., Shusterman, A. A., Lieschke, K. J., Newman, C., & Cohen, R. C. (2018). The Bekeley Atmospheric CO_2 Observation Network: Field calibration and evaluation of low-cost air quality sensors. *Atmospheric Measurement Techniques*, *11*(4), 1937–1946. https://doi.org/10.5194/amt-11-1937-2018

Le Quéré, C., Jackson, R. B., Jones, M. W., Smith, A. J. P., Abernethy, S., Andrew, R. M., & Peters, G. P. (2020). Temporary reduction in daily global CO_2 emissions during the COVID-19 forced confinement. *Nature Climate Change*, *2*, 2. https://doi.org/10.1038/s41558-020-0797-x

Lin, J. C., Gerbig, C., Wofsy, S. C., Andrews, A. E., Daube, B. C., Davis, K. J., & Grainger, C. A. (2003). A near-field tool for simulating the upstream influence of atmospheric observations: The Stochastic Time-Inverted Lagrangian Transport (STILT) model. *Journal of Geophysical Research*, *108*(D16), 4493–4510. https://doi.org/10.1029/2002JD003161

McDonald, B. C., McBride, Z. C., Martin, E. W., & Harley, R. A. (2014). High-resolution mapping of motor vehicle carbon dioxide emissions. *Journal of Geophysical Research: Atmosphere*, *119*, 5283–5298. https://doi.org/10.1002/2013JD021219

Rodgers, C. D. (1990). Characterization and error analysis of profiles retrieved from remote sounding measurements. *Journal of Geophysical Research*, *D5*, 5587–5595. https://doi.org/10.1029/Jd095id05p05587

Shusterman, A. A., Kim, J., Lieschke, K. J., Newman, C., Wooldridge, P. J., & Cohen, R. C. (2018). Observing local CO_2 sources using low-cost, near-surface urban monitors. *Atmosphere Chemistry and Physics*, *18*(18), 13,773–13,785. https://doi.org/10.5194/acp-18-13773-2018

Shusterman, A. A., Teige, V. E., Turner, A. J., Newman, C., Kim, J., & Cohen, R. C. (2016). The BErkeley Atmospheric CO_2 Observation Network: Initial evaluation. *Atmosphere Chemistry and Physics*, *16*(21), 13,449–13,463. https://doi.org/10.5194/acp-16-13449-2016

Turner, A. J., Jacob, D. J., Benmergui, J., Brandman, J., White, L., & Randles, C. A. (2018). Assessing the capability of different satellite observing configurations to resolve the distribution of methane emissions at kilometer scales. *Atmosphere Chemistry and Physics*, *18*(11), 8265–8278. https://doi.org/10.5194/acp-18-8265-2018

Turner, A. J., Köhler, P., Magney, T. S., Frankenberg, C., Fung, I., & Cohen, R. C. (2020). A double peak in the seasonality of California's photosynthesis as observed from space. *Biogeosciences*, *17*, 405–422. https://doi.org/10.5194/bg-17-405-2020

Turner, A. J., Shusterman, A. A., McDonald, B. C., Teige, V., Harley, R. A., & Cohen, R. C. (2016). Network design for quantifying urban CO_2 emissions: Assessing trade-offs between precision and network density. *Atmospheric Chemistry and Physics*, *16*(21), 13,465–13,475. https://doi.org/10.5194/acp-16-13465-2016

Yang, X., Tang, J., Lee, J. E., Rossini, M., Joiner, J., & Richardson, A. D. (2015). Solar-induced chlorophyll fluorescence that correlates with canopy photosynthesis on diurnal and seasonal scales in a temperate deciduous forest. *Geophysical Research Letters*, *42*, 2977–2987. https://doi.org/10.1002/2015GL063201